Clogging of microchannels by nano-particles due to hetero-coagulation in elongational flow

K. Georgieva [a,*], D.J. Dijkstra [b], H. Fricke [c], N. Willenbacher [a]

[a] Institute of Mechanical Process Engineering and Mechanics, Karlsruhe Institute of Technology (KIT), 76131 Karlsruhe, Germany
[b] Bayer MaterialScience AG, 51368 Leverkusen, Germany
[c] Fraunhofer Institute for Manufacturing Technology and Applied Materials Research, Adhesive Bonding and Surfaces, 28359 Bremen, Germany

ARTICLE INFO

ABSTRACT

We have investigated the phenomenon of flow-induced aggregation in highly concentrated colloidal dispersions exposed to strongly converging flow fields. This phenomenon is relevant not only for classical technical operations like coating, pumping or filtration, but also for the application of concentrated suspensions in upcoming processing technologies based on microfluidic devices. A ring-slit device (gap height 10–25 μm), which allows for a variation of flow kinematics in a wide range, has been developed in order to investigate this phenomenon. Various polymer dispersions with different particle surface properties have been used as model systems. Our experiments exclude, that channel clogging is due to retention of pre-existing aggregates, fouling or hydrodynamic bridging. Instead, we demonstrate that clogging of the microchannel is induced by hetero-coagulation between primary colloidal particles and micron-sized impurities present at concentrations on the order of 100–1000 ppm. Clogging can occur even if the diameter of these impurities is less than a tenth of the gap height. Aggregation takes place in the converging flow field at the channel entrance, but not in the shear field within the slit. It can be suppressed by appropriate stabilization of the primary particles.

© 2010 Elsevier Inc. All rights reserved.

1. Introduction

The aggregation of flowing suspensions has a strong impact on the efficiency of many technical processes. It is particularly critical for suspensions exposed to complex flow fields including strong extensional components (converging streamlines) as for example at the entrance to narrow channels. This phenomenon is relevant not only for classical technical operations like coating, pumping or filtration, but also for the application of concentrated suspensions in the upcoming processing technologies based on microfluidic devices.

Aggregation in dilute suspensions at rest (induced by Brownian motion) as well as in simple shear flow has been investigated extensively both experimentally and theoretically [1–5]. Shearing forces can enhance flocculation bringing the particles close enough to collide. Formation of aggregates depends on the interplay between colloidal and hydrodynamic interactions. The relevance of contact time during flow-induced particle collisions for the coalescence and formation of aggregates has been discussed by Chesters [6]. Scattering experiments allow for a determination of aggregation kinetics and aggregate structure and fractal dimension of aggregates depends on the aggregation mechanism as well as on flow conditions [7,8]. Coagulation of high-solid latexes has also been investigated using various light scattering techniques [9,10]. Agitation-induced coagulation of concentrated dispersion has been investigated by Lowry et al. [11]. The authors propose a kinetic model which accounts for the rate of primary particle coagulation and for the coagulation process between large flocs and primary particles. A theoretical study on hetero-coagulation of particles of the same material but different sizes at low shear rates revealed that hetero-coagulation is favored over the respective homocoagulations in the case of coagulation in secondary minimum [12]. Wang reported that in the case of suspensions of different materials and different sizes, the size difference may also induce a secondary shear hetero-coagulation between larger but less stable particles with smaller but more stable particles, if the stability difference is not very large and the particle size difference is not too small.

Although much is known about colloidal stability at rest or in shear flow, little attention has been paid to the process of agglomeration in a suspension subjected to an extensional flow field. Trajectory analysis for dilute suspensions with attractive interactions revealed that the collision rate is dependent on the bulk flow kinematics and stability is higher in shear flow compared with extensional flows under otherwise similar conditions [13]. Zeichner and Schowalter demonstrated that for extensional flow, the

* Corresponding author. Fax: +49 721 608 3758.
E-mail address: kristina.georgieva@kit.edu (K. Georgieva).

hydrodynamic interactions which tend to hinder the approach of colliding particles are less significant [14].

Our study focuses on the aggregation process of electrostatically and/or sterically stabilized highly concentrated dispersions exposed to extensional flow fields. In order to study this phenomenon experimentally we use a ring-slit device, which has already been established to characterize flow-induced aggregation for industrial quality control and product development purposes [15]. This device embodies a capillary viscometer and a ring-slit die. The ring-slit geometry allows us to maintain a small gap height (10–30 μm), corresponding to a high contraction ratio (1:1000), and a large cross-sectional area at the same time. When aggregation takes place the slit entrance is gradually clogged resulting in a strong pressure increase. This method allows for a variation of flow conditions over a wide range. By variation of the volumetric flow rate, slit height and slit entrance angle we are able to control the collision frequency and contact time of colliding particles and the total deformation of a fluid element as well as velocity gradient in the entrance region where aggregation is supposed to takes place.

The clogging phenomenon during suspension flow through narrow channels is an extremely complex phenomenon. Potential mechanisms for clogging of microchannels by flowing colloidal suspension are fouling, i.e. particle deposition as a result of attraction to the wall surface and plugging by aggregation in the flow field or by hydrodynamic bridging. The transport of particles to the wall can be caused by inertial forces, Brownian diffusion, sedimentation and interception. When particles approach a surface to within a fraction of their diameter, surface forces such as van der Waals and electrostatic forces take over. The efficiency of particle attachment is affected by the competition between adhesive and hydrodynamic forces.

A recent experimental study by Wyss et al. [16] concentrated on the blockage mechanism at the level of a single pore using microfluidic channels. They proposed a model based on irreversible sticking of particles near channel constriction when their distance of approach to the wall is comparable to the length scale of the attractive interactions. Wyss et al. showed that a sticking event is determined by the initial streamline on which a particle is travelling and does not depend on flow rate and particle volume fraction.

Hydrodynamic bridging refers to the phenomenon when particles smaller than the channel size arrive simultaneously and block the channel. Hydrodynamic bridging is affected by the colloidal repulsion force and the drag force. The experimental results of Ramachandran and Folger [17] demonstrate that the plugging phenomenon occurs when the flow velocity is higher than a critical velocity and the extent of plugging increases with increasing velocity.

The present study investigates clogging of a microchannel by concentrated suspensions and elucidates the underlying mechanism of flow-induced aggregation. Aggregation is proved not to occur in the pure shear flow within the straight narrow slit. Potential deposition of particles on the slit surface is also considered and it is shown that the clogging phenomenon is not influenced by particle–wall interactions. It will be demonstrated that a small amount of micron-sized objects (e.g. aggregates of primary particles, impurities) extant in concentrated nano-particle suspensions strongly influences the aggregation in a converging flow field. Experimental results demonstrate that the retention of particles at the slit entrance is due to hetero-coagulation between micron-sized objects and primary nano-particles. It will also be shown that the flow-induced aggregation can be controlled by adjusting colloidal particle interactions. Further, this phenomenon depends strongly on the flow rate and the slit clogging is faster the lower the flow rate is. The effect of flow rate is explained with the dynamic balance between aggregation and breakup of aggregates under high shear conditions. Considering an appropriately expressed Breakage number and the aggregation probability based on the interparticle contact time, we will demonstrate that the aggregation efficiency decreases with increasing flow rate, which limits the maximum aggregate size and thus explain the observed flow rate dependence of the slit clogging phenomenon. Furthermore, it will be demonstrated experimentally that smaller slit entrance angles promote the flow-induced aggregation in the ring-slit device. These results will be interpreted with the help of computational fluid dynamic (CFD) simulations, considering the residence time of the particles in the flow field at the slit entrance.

Various polymer dispersions used in coating or adhesive formulations are used here as model systems, but similar phenomena are observed in suspensions of nanosized inorganic, e.g. zinc oxide particles and also in more complex formulations like automotive or paper coating colors [15].

2. Experimental apparatus and procedure

A schematic diagram of the experimental apparatus is shown in Fig. 1a. It consists of a capillary viscometer (Rosand RH2000) and a home-made stainless steel ring-slit die mounted to the bottom end of the wall of a cylindrical sample reservoir. The slit height (H) is varied between 10 and 30 μm and is more than 50 times larger than the mean particle diameter of the nano-particulate suspensions considered here. A well-defined flow kinematics requires perfectly planar wall surfaces of the micrometer slit. Examination of the top and bottom wall surface using a coordinate measuring machine (Zeiss Prismo Navigator) revealed wall planarity within about one micron. It is important to note that the ring-slit die allows for variation of the slit-entrance length (L') and entrance angle (β) as well as the length (L) of the slit itself (Fig. 1b). The technical specifications of our experimental set-up are summarized in Table 1. Flow-induced aggregation and corresponding aggregate retention at the slit entrance are examined by measuring the pressure drop across the ring-slit. The suspension is forced to flow through the ring-shaped slit at a constant volumetric flow rate ($\dot{V}$), which is controlled by setting the piston speed (v). A pressure transducer mounted above the die records the corresponding extrusion pressure (p) as a function of time. If the suspension is stable the pressure adjusts itself to a comparably low constant value determined by the viscosity of the particular sample (Fig. 1c). In this case the instrument operates as a high-shear capillary rheometer and apparent shear rates, $\dot{\gamma}_{app}$, apparent shear stresses, τ_{app}, and viscosity η_{app} can be calculated according to [18]:

$$\dot{\gamma}_{app} = \frac{6\dot{V}}{B \cdot H^2} \quad \text{with} \quad \dot{V} = \pi \cdot R^2 \cdot v \quad \tau_{app} = \frac{p \cdot H}{2L} \quad \eta_{app} = \frac{\tau_{app}}{\dot{\gamma}_{app}} \quad (1)$$

If the suspension is not stable, aggregates gradually clog the slit and the extrusion pressure increases with time. The recorded pressure signal is normalized by the so-called viscous pressure (Pviscous), the initial pressure reading that corresponds to the viscosity of the particular sample, so that we only compare the pressure increase caused by the aggregate retention. All experiments are conducted at room temperature.

It should be mentioned that the slit height was determined indirectly by calibration measurements with standard silicon oil (Wacker Chemie AG, Germany) of known viscosity (η = 0.01 Pa s), which behaves as a Newtonian fluid at the shear rates applied (1300–5000 s^{-1}). Knowing the slit length and width, the piston speed and viscosity of the used silicon oil, the slit height is easily obtained from Eq. (1).

All samples are pre-filtered prior to the ring-slit tests in order to remove impurities and aggregates formed in previous processing
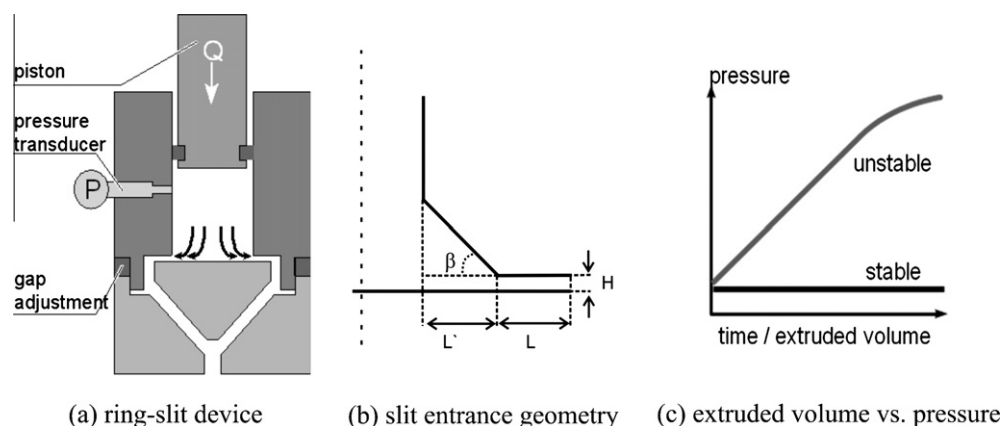
(a) ring-slit device (b) slit entrance geometry (c) extruded volume vs. pressure

Fig. 1. Ring-slit device (a), details of the slit entrance geometry (b) and pressure development for stable and unstable samples (c).

Table 1
Technical specifications of the ring-slit device.

Specification	Value
Radius R of cylindrical sample chamber	12 mm
Gap height H	11 μm, 21 μm and 26 μm
Entrance gap width $B = 2\pi R$	62.8 mm
Gap length L	1 mm and 0.8 mm
Entrance length L'	1 mm and 1.2 mm
Entrance angle α	30°, 45° and 90°

steps. Aiming at qualitative and quantitative characterization of these micron-sized objects present in the dispersions, the investigated nanosuspensions have been analyzed by means of a single-particle optical sensing technique (SPOS) counting individual objects. The used SPOS instrument used is an AccuSizer 780A (PSS, Inc., Santa Barbara, CA) equipped with a model LE400-05ES particle sensor. The optical sensor is factory calibrated using size-certified polystyrene standards. Particle size distributions can be measured in the diameter range of 0.5–400 μm and particle concentration in the range of 10^4–10^5 particles/cm³. It should be noted that correction for the effect of refractive index has not been considered, since the refractive index for the analyzed latexes (1.54 for polyurethane and 1.56 for polychloroprene) is only slightly smaller than the refractive index of the polystyrene latex (1.59) used for the calibration. Moreover, the refractive index has been shown to account for differences in the particle size only in the lower detection limits (particles smaller than 1 μm).

Data collection was provided by the CW788-Nicomp software (PSS, Inc., Santa Barbara, CA), which accumulate the data in 512 logarithmically spaced channels from minimum to maximum size. The evaluation of raw particle counts per size channel allows for calculation of measured particle volume. Accordingly, by measuring a defined amount of the suspension the volume fraction of micron-sized particles can be obtained. This technique is especially suitable for detecting and characterizing small fractions of objects larger than the primary particles [19].

Shear flow aggregation experiments were performed using a rotational rheometer RS-150 (ThermoHaake, Germany) equipped with a double concentric cylinder shear cell (DIN 5344). The inner and outer radii of the stator are 42.8 mm and 43.4 mm, respectively, while the values for the rotor are 35.5 mm and 36.0 mm. This results in an inner and outer gap width of 50 μm. The shear rate employed was in the range of 10–8000 s⁻¹. For determination of agglomerate size, the samples taken after the shear experiment were gently withdrawn from the tank into the AccuSizer container using a pipette. The same procedure was used with the samples after the ring-slit experiments in order to determine the size distribution and volume fraction of aggregates after experiments at different flow rates.

3. Colloidal systems and sample preparation

Three highly concentrated aqueous latex dispersions are used as model colloids. The characteristics of the investigated samples are summarized in Table 2. The polyurethane and polychloroprene dispersion were supplied by Bayer MaterialScience as raw materials. A polystyrene dispersion was provided by Dow Chemical Company. The suspensions investigated here are designed for a shelf-life of more than 6 months. According to the manufacturer, the polyurethane dispersion is synthesized by solution polymerization and subsequent precipitation without the use of surfactants [20]. The polyurethane particles are electrostatically stabilized by surface charges due to ionized sulfonate groups. In the case of the polychloroprene particles the surface charge arises from adsorbed surfactant molecules with carboxylic groups. Information about the chemical nature of the surface charge of the commercial polystyrene particles is not available. The range of the interaction potential (Debye-Hückel length) was estimated by mapping the divergence of the zero-shear viscosity onto that of hard sphere dispersions [2].

Photon correlation spectroscopy was used to determine the size distribution of the particles. The average diameter of the particles is about 140 nm in the case of the polyurethane (PU) and polystyrene (PS) particles and about 100 nm in the case of the polychloroprene particles. The width of the particle size distribution is about ±20% of the average size for all three systems.

The polymerization process during manufacturing of latex dispersions often involves formation of aggregates or particles larger than the primary particles. These impurities account only for a small fraction of the total particle content in the order of 100 ppm. But these large particles or agglomerates which are

Table 2
Properties of the investigated dispersions.

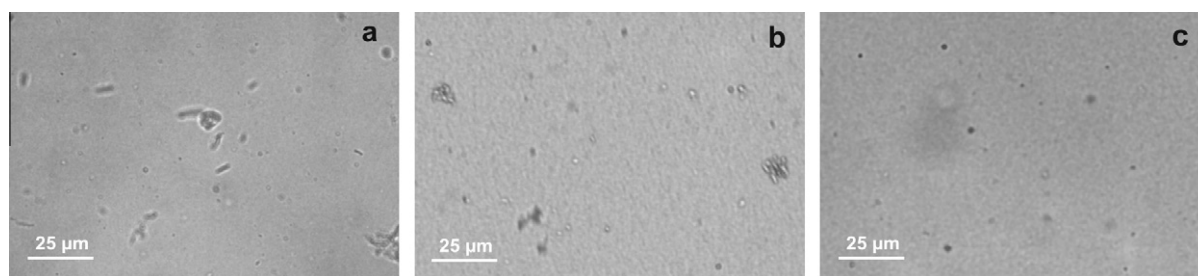| Property	Polychloroprene	Polyurethane	Polystyrene
Solids content (wt.%)	49	43	48
Glass transition temperature (°C)	−40	−40	95
Mean particle diameter (nm)	100	135	140
pH	12	7	6
Debye–Hückel length (nm)	2	8	2
Zeta potential (mV)	−62	−56	−59

Fig. 2. Light microscopy image showing aggregates in coarse pre-filtered PU (a), PS (b) and polychloroprene dispersion (c).

almost unavoidable in technical manufacturing processes for nano-particle suspensions play a crucial role in flow-induced aggregation, as will be shown below. Therefore, we have characterized this fraction carefully as described in the following section.

Light microscopy observations revealed that the PU and PS dispersions contain predominantly elongated and irregular agglomerates, in contrast to the polychloroprene dispersion which contains smaller but mainly spherical micron-sized particles (Fig. 2). It should be noted that we use the term micron-sized particles for all objects larger than the primary particles without knowing their origin.

Dispersions were always pre-filtered prior to ring-slit experiments using synthetic woven monofilament fabrics purchased from Sefar AG with mesh size 1 μm (Sefar PETEX) and 25 μm (Sefar NITEX). Pre-filtration was performed very gently using large filters to maximize the filtration area. Due to the irregular shape of the micron-sized particles in the investigated dispersions it was difficult to control the filtration efficiency. Thus, in this paper, the filter with 1 μm mesh size is referred to as a "fine filter" and correspondingly the "25 μm filter" as a "coarse filter".

The quantitative characterization of pre-existing aggregates with respect to filtration was provided by SPOS measurements. Fig. 3a shows the volume distribution results for the PS dispersion and Fig. 3b for the PU and polychloroprene dispersion. These data quantitatively confirm that the micron-sized particles in the coarse pre-filtered PU and PS dispersions have a median diameter (d_{50}) of 9 μm and 6 μm respectively, whereas the micron-sized particles in the polychloroprene dispersion are smaller (d_{50} = 1.5 μm). The effect of pre-filtration is evident for the PU and PS dispersions but it has no significant effect on the polychloroprene dispersion.

It should be noted that the measured diameter in the case of PU and PS is rather overestimated due to the irregular, predominantly elongated shape of micron-sized particles. The laminar flow through the optical sensor causes the longest particle dimension to be aligned with the direction of the flow, thus the observed particle size is related to a projected area containing the long axis and is displayed as an equivalent sphere diameter.

The SPOS technique was also used to determine the volume fraction of the measured aggregates with respect to the filtration efficiency of the different filters. The results are reported in Table 3. The effect of filtration is again evident for the PU and PS suspension. It can be also seen that the highest volumetric concentration of micron-sized particles is present in the PS suspension.

Monodisperse PMMA particles with diameters of 1, 10 and 14.5 μm have been used in hetero-coagulation experiments. The PMMA particles of 1 μm diameter are electrostatically stabilized by surface charges due to ionized sulfate groups. The electrokinetic
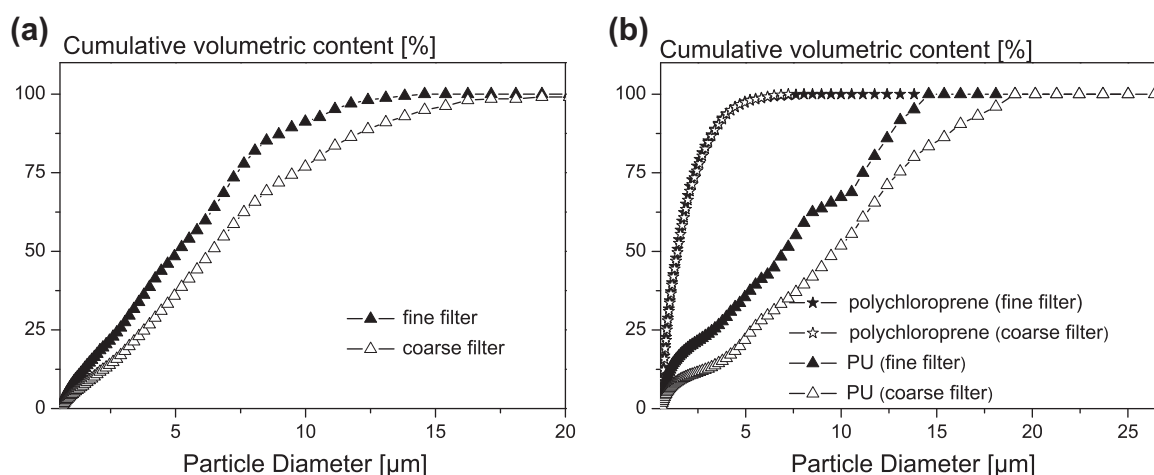

Fig. 3. Cumulative volumetric distribution of micron-sized particles in PS (a) and PU and polychloroprene (b) from the measurements using AccuSizer 780A.

Table 3
Quantitative analysis of aggregate fractions in the investigated PU, PS and polychloroprene dispersions.

	PU		Polychloroprene		PS	
	Coarse filter	Fine filter	Coarse filter	Fine filter	Coarse filter	Fine filter
Volume fraction of aggregates (ppm) ($V_{aggregates}/V_{dispersion}$)	204	80	47	37	365	240
Number of aggregates $\geqslant 1$ μm (10^6 aggregates/ml$_{dispersion}$)	4.6	4.2	16	14	24	22

surface charge was determined to be 0.0169 meq/g by means of particle-charge detector (Mütec PCD 03), in combination with an automatic titration unit (DL 25, Mettler Toledo). According to the manufacturer the PMMA particles of 10 μm and 14.5 μm diameter are stabilized by polyvinylalcohol adsorbed on the particle surface. Measurements with the particle-charge detector confirmed that these particles are not charged.

In order to investigate the effect of surfactants on dispersion stability, two types of surfactant, an anionic and non-ionic surfactant, were used. The anionic sodium dodecyl sulfate (Carl Roth Ltd., Germany) has a molar mass of 288 g/mol and provides a thin stabilizing layer owing to the small size of the SDS molecule. The SDS molecules contain 12 carbons and the length of a molecule in the stretched configuration is only about 1.7 nm [21]. The non-ionic polymeric surfactant is based on stearyl alcohol polyglycol ether (TANATEX Chemicals, Germany) and contains polymer chains of different lengths. According to the manufacture the average molar mass amounts to 1240 mol/g.

4. Experimental results and discussion

4.1. Clogging mechanism

The purpose of this investigation is to reveal the aggregation mechanism causing the clogging of narrow gaps when concentrated polymer dispersions are processed in elongational flow fields. We use the ring-slit device for this study according to the procedure described above and in this first section we focus on the effect of flow rate and particle wall interactions.

Particle deposition could be a possible mechanism for clogging of microchannels by flowing nanosuspensions. The adhesive forces and corresponding deposition efficiency depend on the hydrophobic/hydrophilic interactions between particles and wall surface. Particle deposition at the wall was examined using two slit dies with different surface properties: one plain stainless steel slit, which is hydrophilic in nature and a second one covered with a 2 μm thin silicon based hydrophobic film (Toposeal, MSTagion). The results for the coarse pre-filtered PU suspension at a slit height of 21 μm are presented in Fig. 4 for 314 mm^3/s (Fig. 4a) and 63 mm^3/s (Fig. 4b) volumetric flow rate. We observe similar pressure increase as a function of extruded volume for the same hydrodynamic conditions. This finding suggests that the particle–wall colloidal interactions are irrelevant for the mechanism of slit clogging and particle deposition is insignificant for the chemical and

physical conditions investigated here. This is further supported by the following considerations: the stainless steel has an isoelectric point close to 5.5–6 and at higher pH it is negatively charged [22]. Hence, in the pH range relevant for the investigated dispersions, the electrostatic interactions between the negatively charged latex particles and the stainless steel are repulsive and deposition on the wall is rather unlikely.

Fig. 5 shows the effect of flow rate on particle retention for three different suspensions. In all experiments the Reynolds number for suspension flow in the slit entrance region and within the microchannel is very small (Re < 1). Results for the PU suspension (coarse pre-filtration), obtained at a slit height of 21 μm are shown in Fig. 5a. Similar experiments were performed with the polychloroprene dispersion but the gap height was set to 11 μm (Fig. 5b). In both cases the experiments were done using a slit die with a 45° entrance angle. The effect of flow rate on the stability of the polystyrene dispersion (coarse pre-filtration) is demonstrated in Fig. 5c. For this data we used a ring-slit die with a 30° slit entrance angle and we fixed the slit height at 26 μm. Although the absolute values of the normalized pressure are very different for the three dispersions the results presented in Fig. 5 shows a strong flow rate dependence. The pressure increase is most pronounced when the samples are extruded at the lowest piston speed. A continuous decrease of the normalized pressure drop is detected when increasing the flow rate. These results show that we indeed observe a flow-induced phenomenon; simply collecting pre-existing objects larger than the gap height would only depend on the total amount of extruded volume but not on the flow rate. Moreover, this flow rate dependence excludes plugging by hydrodynamic bridging for which the extent of slit clogging should increase with increasing flow rate [17].

The results from repeated extrusion of the coarse pre-filtered PU dispersion through the ring-slit device at constant flow rate showed no significant change in the pressure increase, further confirming that clogging by straining can be neglected.

The extruded volume of the coarse pre-filtered PU suspension has been analyzed using the SPOS technique. The relative amount of aggregates found at different flow rates is given in Table 4. The amount of aggregates in the extruded sample decreases with increasing flow rate. In fact, at the lowest flow rate, a considerable increase in the agglomerate volume fraction in comparison to the sample before the ring-slit test is found, which reveals that not all the aggregates formed during flow are collected at the gap entrance. On the other hand at the highest flow rate we detected a
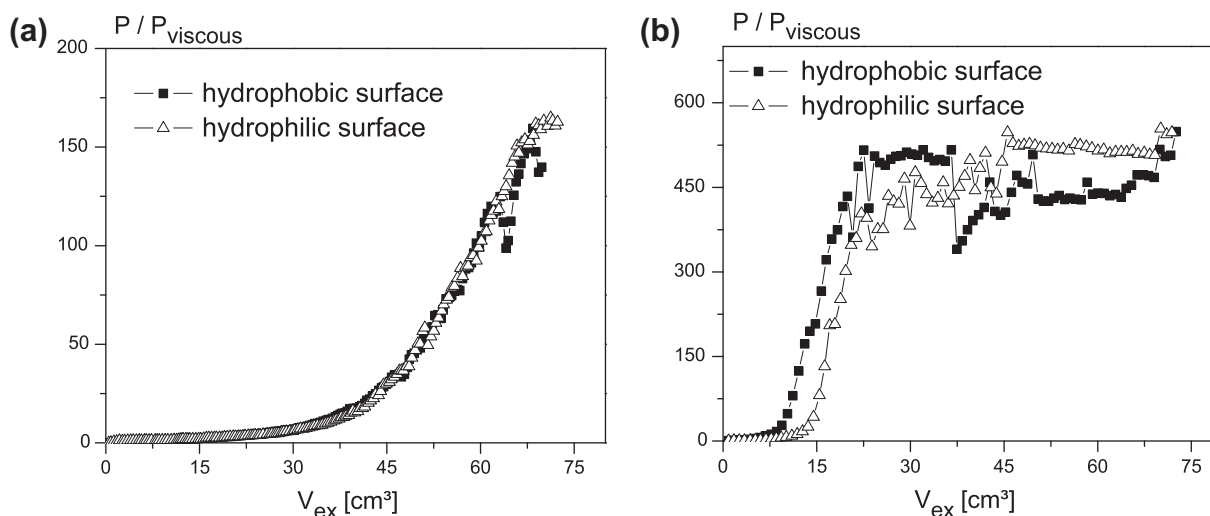

Fig. 4. Effect of surface hydrophobicity on the clogging phenomenon in the ring-slit device for the PU dispersion (coarse filter, ϕ = 0.4, H = 21 μm, β = 45°) at 314 mm^3/s (a) and 63 mm^3/s flow rate (b).
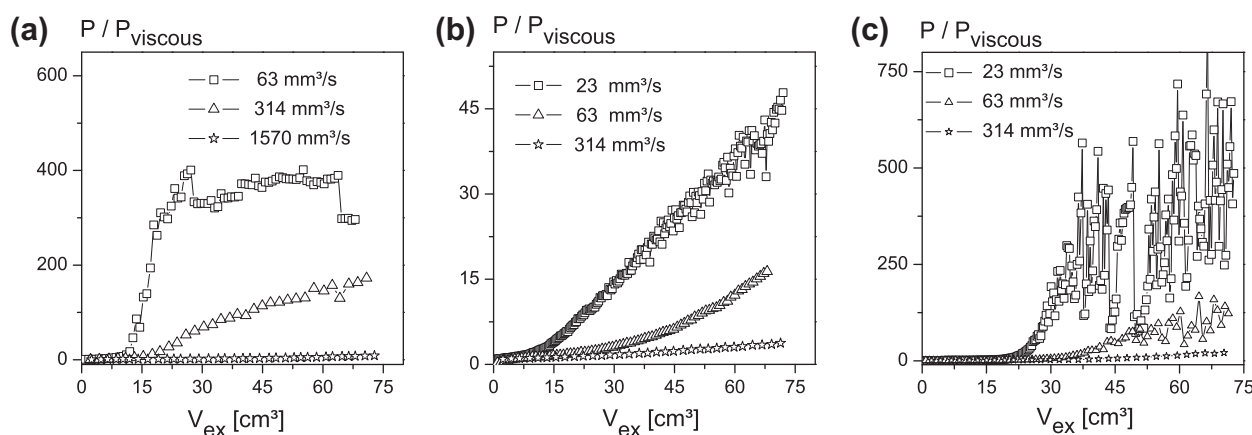
Fig. 5. Effect of flow rate on the flow-induced aggregation of coarse pre-filtered PU dispersion at ϕ = 0.4, H = 21 μm and β = 45° (a), coarse pre-filtered polychloroprene dispersion at ϕ = 0.44, H = 11 μm and β = 45° (b) and coarse pre-filtered PS dispersion at ϕ = 0.47, H = 26 μm and β = 30°.

decrease in the aggregate volume fraction, which can be attributed to the breakup of pre-existing aggregates at these particular hydrodynamic conditions. At the intermediate flow rates the volume fraction of aggregates in the extruded dispersion remains almost unchanged. These results support the notion that the observed clogging phenomenon is a result of flow-induced aggregation, which is most pronounced at the lowest flow rates investigated here (see Table 4).

Since flocculation of particles within the slit channel is also possible, we tested dispersion stability in a pure shear flow using a concentric cylinder shear cell. The samples were sheared for 15 min at different shear rates between $10\,s^{-1}$ and $8000\,s^{-1}$. During these experiments the suspensions are exposed to the shear field orders of magnitude longer than in the ring-slit experiments, but no significant increase in the number or size of aggregates due to shear could be observed. The measured volume fraction of aggregates in the PU dispersion even decrease by about 25% for shear rates higher than $100\,s^{-1}$. It should be noted that the shear rate in the slit channel at the lowest piston speed applied in our experiments corresponds to $6700\,s^{-1}$, which is comparable to the shear rate applied in the shear cell. Hence aggregate formation in the simple shear flow within the slit channel is unlikely and is therefore not a factor in the experiments. Aggregate formation in the complex flow field at the slit entrance and subsequent retention of the aggregates larger than the slit height is most likely to be the dominant mechanism in the ring-slit test. Indeed, a large amount of coagulum is found at the slit entrance after extrusion experiments in which a marked pressure increase was observed.

4.2. Hetero-coagulation in elongational flow

In the materials section we have shown (Fig. 3 and Table 3) that all the dispersions investigated here contain a small amount of mi-

Table 4
Quantitative analysis of aggregates in the extruded PU dispersion (coarse pre-filtered) at different flow rates (H = 21 μm and α = 45°).

Flow rate (mm³/s)	Volume fraction of aggregates ($V_{aggregates}/V_{dispersion}$) (ppm)
Unsheared	204 ± 20
23	340
63	216
314	196
1570	160

Table 5
Maximal length of the region of velocity increase derived by simulation.

Percentage of maximal velocity (%)	30°	45°	90°
20	200 μm	140 μm	80 μm
40	79 μm	57 μm	39 μm

cron-sized particles. The impact of these objects on flow-induced aggregation will be discussed next.

Fig. 6a shows the effect of pre-filtration for the PU suspension at 314 mm³/s volumetric flow rate, and it is apparent that the pre-filtration has a dramatic effect on the clogging phenomenon. Similar data obtained for the PS suspension at 63 mm³/s are shown in Fig. 6b. The trend is the same for lower as well as higher flow rates. These results show that the amount and size of impurities strongly influences the clogging mechanism. We should also mention that the polychloroprene dispersion which contains smaller agglomerates proved to be stable for the 21 μm slit over the whole flow rate range.

As already mentioned the irregular form of micron-sized objects strongly influences the filtration efficiency and makes it difficult to control the size and amount of aggregates. We therefore added monodisperse PMMA particles of a defined size and concentration to the fine pre-filtered PU dispersion, in order to investigate systematically the effect of impurities on the flow-induced aggregation. For comparison the homocoagulation of PMMA particles in the ring-slit device was also tested by conducting experiments with PMMA particles dispersed in an aqueous glycerine solution with the same viscosity as the PU dispersion. Fig. 7 shows the effect of PMMA particles on the flow-induced aggregation for the fine pre-filtered PU suspension. The data in Fig. 7a refers to a particle concentration of 100 ppm (relative to the total dispersion volume) and those in Fig. 7b to 1000 ppm particle concentration. It is evident from this plot that the PMMA dispersion itself is stable in the converging flow field, as we observe a constant pressure signal. However, when the same amount of PMMA particles is dispersed in the PU suspension a significant pressure increase is detected. The implication of these results is that slit clogging is due to the hetero-coagulation of PU and PMMA particles.

Further evidence for hetero-coagulation is provided by electron micrographs of the coagulum retained at the slit entrance after experiments with 100 ppm and 1000 ppm of 10 μm PMMA particles dispersed in the PU dispersion, as shown in Fig. 8. The continuous indistinguishable mass that we see on the images is created by aggregated PU particles which are soft and deformable at room
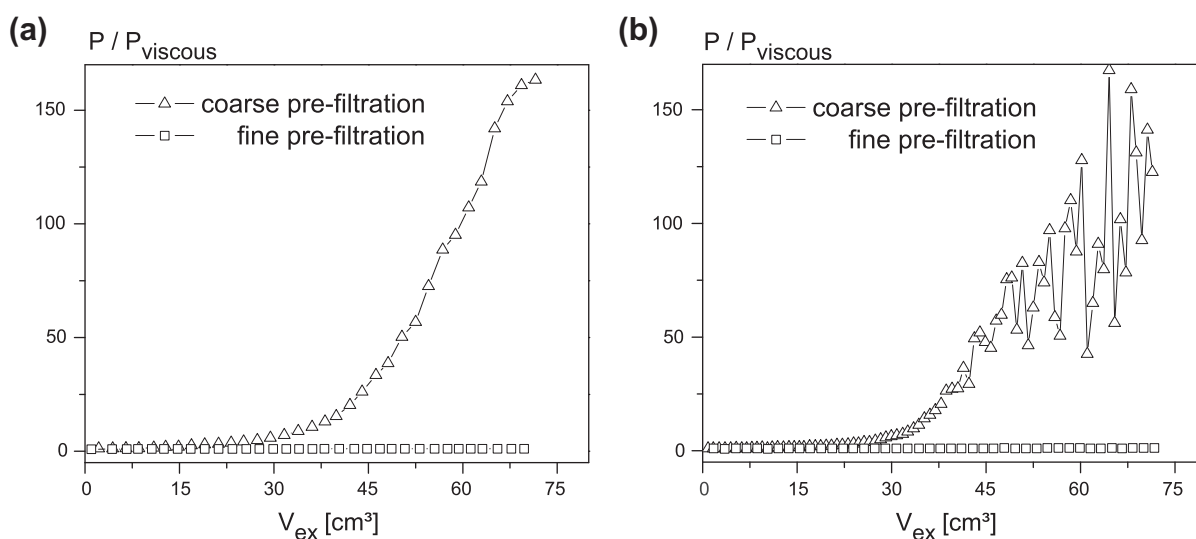
Fig. 6. Effect of micron-sized particles on the flow-induced aggregation of (a) PU dispersion ($\phi = 0.4$, $H = 21$ μm, $\beta = 45°$ and flow rate = 314 mm^3/s) and (b) PS dispersion ($\phi = 0.47$, $H = 25$ μm, $\beta = 30°$ and flow rate = 63 mm^3/s).
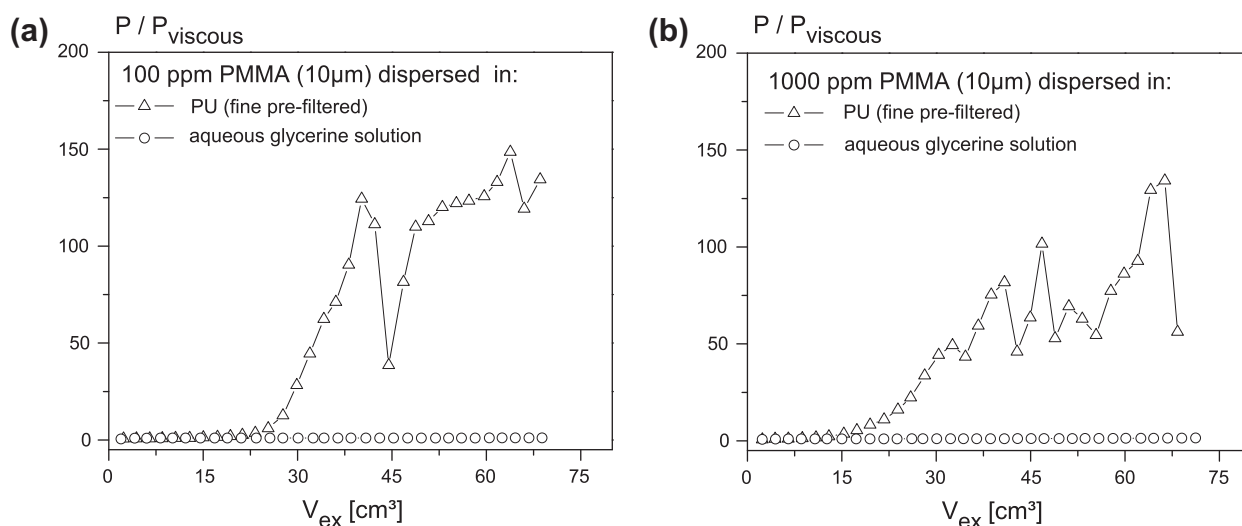

Fig. 7. Effect of 10 μm PMMA particles on the flow-induced aggregation of PU dispersion at 100 ppm PMMA (a) and at 1000 ppm PMMA particles ($\phi = 0.4$, $H = 21$ μm, $\beta = 45°$ and flow rate = 314 mm^3/s).

temperature due to the very low glass transition temperature (-40 °C). In contrast to the PU particles, the PMMA particles are hard at room temperature and appear as spheres on the micrographs. These images confirm that the coagulum which clogs the slit consists of PMMA as well as PU particles.

In Fig. 9a the effect of PMMA particle size is represented for three different particle sizes (1 μm, 10 μm and 14.5 μm diameter). In these experiments the volume fraction of PMMA particles is fixed at 100 ppm and the hydrodynamic conditions are the same as in the experiments described above. It is evident that the size of the PMMA particles has no significant effect on dispersion stability. The strong pressure increase observed with the 1 μm particles is especially striking since these particles are twenty times smaller than the gap of the ring-slit. Fig. 9b demonstrates the dependence of the PU suspension stability on the amount of 1 μm PMMA particles. It can be seen that the rate of slit clogging decreases with decreasing PMMA particle volume fraction. Obviously a critical amount of PMMA particles is required to induce the clogging phenomenon.

Fig. 10a shows the dependence of polychloroprene flow stability on the PMMA particle size. For these experiments 1000 ppm PMMA particles were dispersed in the suspension and the samples were extruded through a 21 μm slit at a flow rate of 314 mm^3/s. A clear effect of PMMA particle size on polychloroprene stability can be seen in this case and the pressure increase is more pronounced as the ratio of particle size to gap width decreases. Despite the high PMMA particle concentration the magnitude of the normalized pressure in these experiments is much smaller than that for the PU suspension shown in Fig. 9a. The implication of this result is that the polychloroprene particles are better stabilized than the PU particles and the aggregation efficiency between PMMA and polychloroprene particles is greatly reduced, which is actually a further argument for the hetero-coagulation mechanism in the ring-slit device. The effect of the PMMA particle volume fraction on the flow-induced aggregation of the polychloroprene dispersion is demonstrated for the 14.5 μm PMMA particles in Fig. 10b. As expected, normalized pressure decreases with decreasing PMMA particle volume fraction.
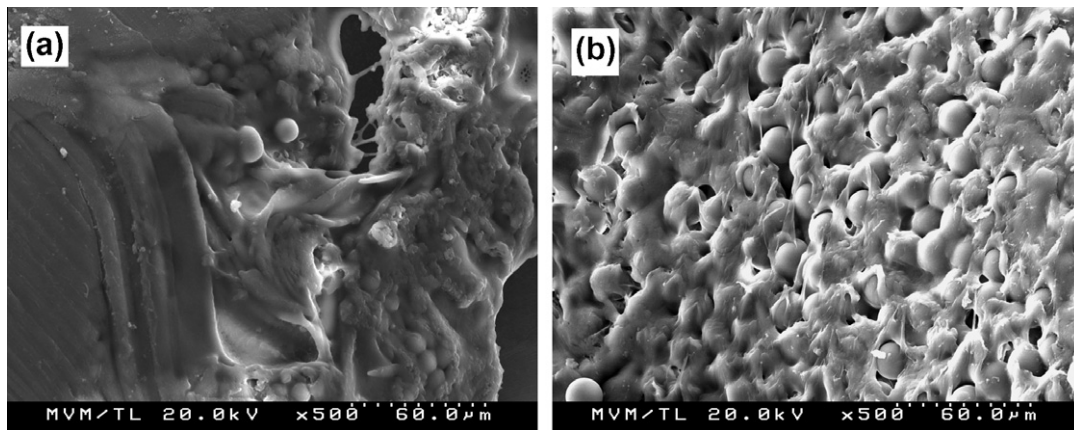
Fig. 8. Electron micrographs of the coagulum after the ring-slit test of aPU-dispersion with (a) 100 ppm PMMA and (b) 1000 ppm PMMA particles (10 μm).
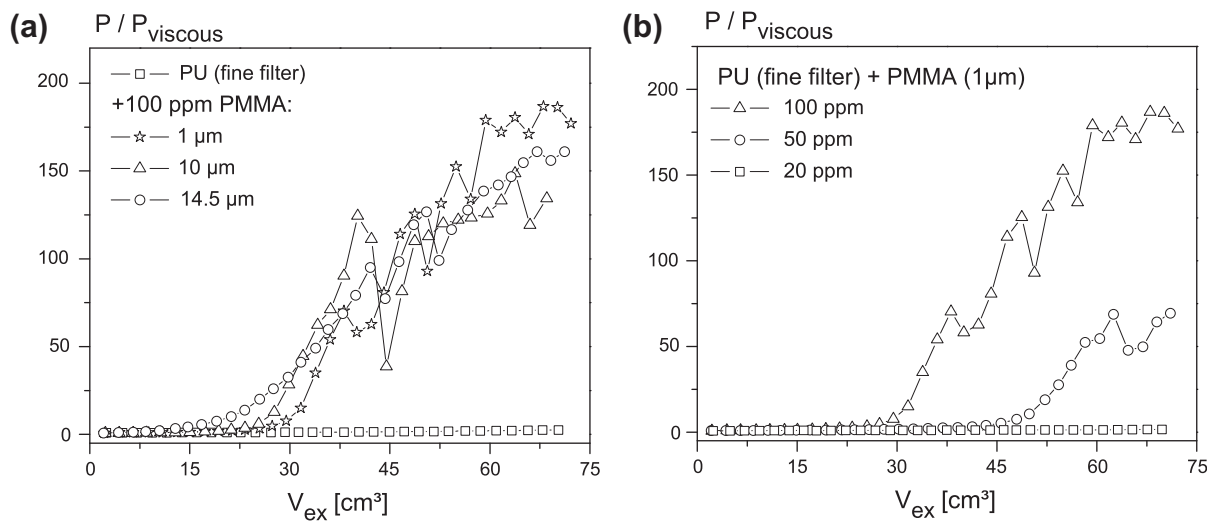

Fig. 9. Effect of PMMA particles size (100 ppm) (a) and PMMA particle (1 μm) volume fraction (b) on the flow stability of the PU dispersion (fine filter, $\phi = 0.4$, $H = 21$ μm, $\beta = 45°$ and flow rate = 314 mm^3/s).
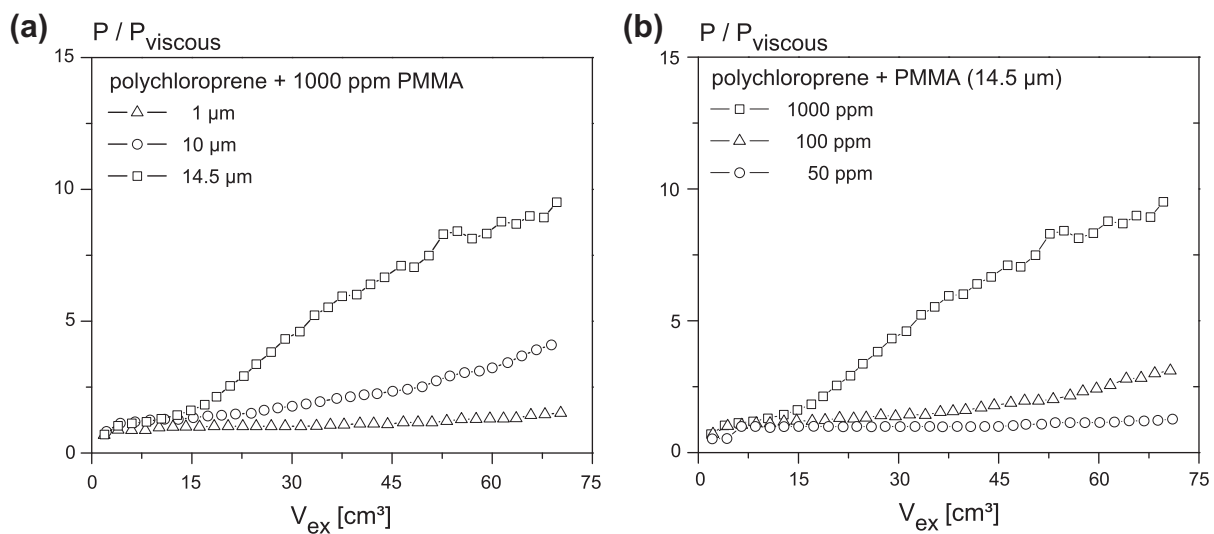

Fig. 10. Effect of PMMA particles size (1000 ppm) (a) and PMMA (14.5 μm) particle volume fraction (b) on the flow-induced aggregation in the polychloroprene suspension (fine filter, $\phi = 0.44$, $H = 21$ μm, $\beta = 45°$ and flow rate = 314 mm^3/s).

Fig. 11 shows the effect of PU particle concentration on particle retention for a 21 µm slit and constant volumetric flow rate (314 mm³/s). In these experiments the polyurethane dispersion was coarse pre-filtered and diluted to different concentrations using KCl solution (0.01 M). The normalized pressure drop across the slit is plotted as a function of the volume of particles extruded (Vex ∗ ϕ). Obviously the data obtained for different particle volume fraction superimpose very well, which means that slit clogging is controlled by the total number of particles that have passed the slit, but the efficiency of particle retention does not depend on the particle concentration. Similar results are obtained for both lower and higher flow rates. These results can be explained by the hetero-coagulation between micron-sized particles and primary particles. Since the number of primary particles is infinite in comparison to the micron-sized particles, hetero-coagulation should depend linearly on the concentration of micrometer objects, assuming that the aggregation efficiency is high enough. Furthermore, the linear dependence on particle volume fraction indicates that hetero-coagulation predominates over the coagulation of the aggregates themselves, for which the aggregation rate should be proportional to the second power of concentration. Finally, clogging by particle–wall interactions or size exclusion could also explain the linear concentration dependence of the pressure increase but all experimental results presented above confirm that these phenomena are not relevant for the experiments discussed here.

4.3. Impact of colloidal particle properties on flow-induced aggregation

The emphasis in this section is placed on the influence of the colloidal properties of the nano-particles which play a crucial role in dispersion stability. To prevent flowing particles from agglomerating, the repulsive potential barrier should be such that the hydrodynamic forces cannot overcome it. In order to investigate the impact of colloidal particle interactions, we tested the effect of surfactant adsorption and ionic strength on the flow-induced aggregation.

The adsorption of surfactant molecules on colloidal particles provides steric and electrostatic repulsion depending on the surfactant type. The influence of the surfactant on the flow-induced coagulation of the PU dispersion (coarse pre-filtration) was studied for an an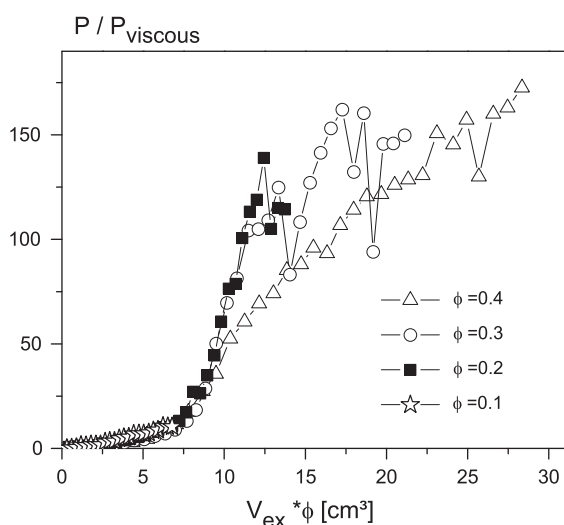ionic SDS surfactant and for a non-ionic surfactant based on polyglycol ether. Fig. 12a shows the effect of the SDS surfactant for three different concentrations at a flow rate of 314 mm³/s and a slit height of 21 µm. These data demonstrate that flow stability increases upon addition of SDS in the range of 11–27 mmol/l (referred to the volume of dispersion medium). With increasing SDS concentration, both the repulsive steric potential energy and the electrical double layer repulsion are increased, leading to a decrease in particle aggregation efficiency. When the surface is fully covered the hydrodynamic forces cannot overcome the repulsive potential and the dispersion is stable [23]. Indeed, we have estimated that at 27 mmol/l surfactant concentration all the primary PU particles are fully covered. A similar effect of the SDS surfactant on flow-induced aggregation was obtained for the PS dispersion as well as for the PU suspension in the presence of PMMA particles. Fig. 12b shows that the non-ionic polymeric surfactant also improves the flow stability of the coarse pre-filtered PU suspension. The PU particles are entirely covered by the non-ionic surfactant at lower surfactant concentration due to the much lower critical micelle concentration in comparison to that of SDS surfactant.

The thickness of a surfactant layer relative to the particle size is an essential factor for an effective steric stabilization. Since the van der Waals attraction force is proportional to particle size, larger particles will need thicker stabilizing layers to prevent the approach of the particles within the range of the attractive van der Waals forces [2]. The attractive force between two 1 µm particles is higher by a factor of 10 than that experienced between 100 nm particles at a given particle surface separation. Typically a surfactant layer thickness of a tenth of the particle radius is needed to prevent irreversible particle aggregation [2,24,25]. Accordingly, effective steric stabilization of the large micrometer aggregates by the relatively small surfactant molecules is very unlikely. Therefore, we can argue that the improved stability of the primary nano-particles due to the added surfactant reduces the flow-induced aggregation. This further supports the idea of hetero-coagulation.

Another important factor which influences dispersion stability is ionic strength. Dialysis against salt solutions of defined ionic strength allows us to tune the range of electrostatic repulsion. As expected, experiments with the dialysed PU suspension (data not shown here) revealed, that the pressure increase is more pronounced for higher ionic strengths, when the range of electrostatic repulsion potential is smaller due to the compression of the electrical double layer.

4.4. Interpretation of the effect of flow rate on flow-induced aggregation

In the previous sections we have experimentally demonstrated that the slit clogging is due hetero-coagulation in the converging flow field at the slit entrance and the slit clogs faster the lower the flow rate is (Fig. 5). In this section we will consider the agglomeration and the agglomerate breakage mechanism under high shear conditions in order to gain a better understanding of the effect of flow rate.

Flow-induced agglomeration of strongly repulsive particles requires that the hydrodynamic force acting on particles is high enough to overcome the repulsive interaction energy barrier (U_{max}). In a recent work, Zaccone et al. pointed out that a critical Peclet number exists [26], $Pe_c = U_{max}/(2\alpha k_B T)$, where $k_B T$ is the thermal energy and α is a coefficient which accounts for the flow kinematics. The basic idea is that when the Peclet number of the sheared suspension is greater than Pe_c, the shearing energy is higher than the energy barrier provided by the colloidal forces and the aggregation process is activated, otherwise the aggregation process is reaction limited and very slow.
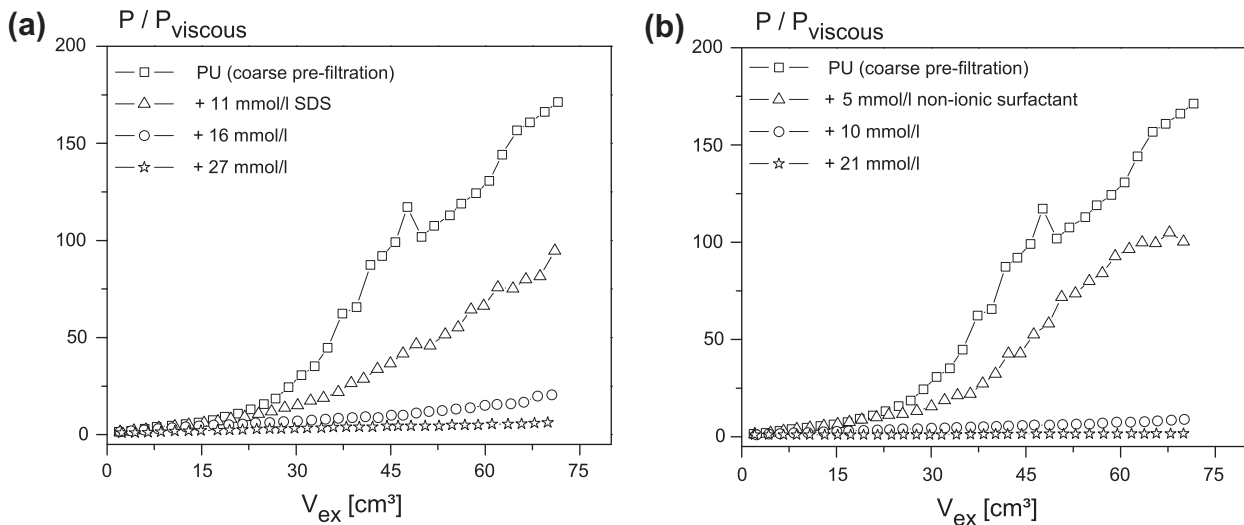

Fig. 11. Effect of volume fraction on the clogging phenomenon for the PU dispersion (coarse filter, H = 21 µm, β = 45° and flow rate = 314 mm³/s).

Fig. 12. Effect of anionic SDS surfactant (a) and non-ionic polymeric surfactant (b) on the flow stability of PU dispersion (coarse filter, $\phi = 0.4$, $H = 21\ \mu m$, $\beta = 45°$ and flow rate = 314 mm^3/s).

We estimated U_{max} from the total colloidal interaction energy, according to the classical DLVO theory. The electrostatic repulsive potential (U_R) was computed using the modified Hogg–Healy–Fuersteneau approximation derived by Sader et al. [27]:

$$U_R = \frac{4\pi\varepsilon_r\varepsilon_0 a\psi_s^2}{l} \ln[1 + \exp(-\kappa a(l-2))] \tag{2}$$

where l is the dimensionless interparticle separation defined as the ratio between center-to-center separation (r) and particle radius (a), ε_r the relative dielectric constant of the dispersion medium, ε_0 the permittivity of vacuum. The surface potential ψ_s is assumed to be equal to the measured zeta-potential and the Debye length κ was set to the values estimated rheologically as reported in the material section. For the van der Waals attractive potential we used the expression reported in [2], which considers the interaction of spherical particles of different radius:

$$\Psi_{vdW} = -\frac{A_H}{6}\left[\frac{2a_1 a_2}{r^2 - (a_1 + a_2)^2} + \frac{2a_1 a_2}{r^2 - (a_1 - a_2)^2} + \ln\frac{r^2 - (a_1 + a_2)^2}{r^2 - (a_1 - a_2)^2}\right] \tag{3}$$

The value of the Hamaker constant (A_H) is assumed to be equal to the one for polystyrene (1.3×10^{-20} J) for all of the investigated colloidal systems. Using the estimated U_{max} values and setting the coefficient α equal to 0.19, by assuming an axisymmetrical extensional flow [28], we obtain the corresponding critical Peclet number values, which are Pe$_c$ = 758, 689 and 592 for the PU, PS and polychloroprene suspension respectively.

In order to compare the Peclet number for our experimental conditions with Pe$_c$, we have calculated the Peclet number for homocoagulation (Pe = $6\pi\eta a_p^3\dot{\gamma}/k_B T$), where a_p is the radius of the primary nano-particles, and for hetero-coagulation (Pe$_{p,i}$ = $3\pi\eta\dot{\gamma}(a_p + a_i)a_p a_i/k_B T$), where a_i is the radius of the micron-sized impurities. For a_i = 1 μm and a_p = 70 nm the obtained Pe and Pe$_{p,i}$ values are 77 and 8412 respectively, at the slit wall shear rate, $\dot{\gamma}$ = 4900 s^{-1}, corresponding to the lowest flow rate (23 mm^3/s). Thus, the critical Peclet number is exceeded for all investigated systems if micron-sized impurities are present in the suspension, which supports the notion of hetero-coagulation evidenced by the experimental results (Figs. 8–11). Furthermore, these considerations suggest formation of aggregates even, e.g. for the fine pre-filtered samples. Indeed, SPOS analysis of the fine pre-filtered PU dispersion after extrusion at the lowest flow rate revealed an in-

crease in the agglomerate volume fraction in comparison to the sample before the ring-slit test, although the slit was not clogged. On the other hand, Pe$_{p,i}$ increases also when increasing the shear rate, suggesting that the particle aggregation should become more likely at high flow rates, which is in contradiction with the results shown in Fig. 5. The effect of flow rate on the slit clogging can be understood considering the effect of interparticle contact time on the aggregation probability and the process of aggregate breakage leading to a reduction of the maximum aggregate size.

Chesters argued that the aggregation probability depends not only on the collision force but also the collision duration [6]. He pointed out that the time ($t_{contact}$) spent by two particles in immediate vicinity is inversely proportional to the shear rate and aggregation will occur if the contact time exceeds the time ($t_{drainage}$) required for drainage of the fluid in the small gap between approaching particles to a critical separation ($h_c \sim (A_H/72\pi\eta a\dot{\gamma})^{1/2}$) at which the van der Waals attraction becomes comparable with the hydrodynamic force. Hence, the aggregation probability (P), providing first indication of whether approaching particles will stick together or not, can be expressed as an exponential probability function of the ratio between $t_{drainage}$ and $t_{contact}$:

$$P \approx \exp\left(-\frac{t_{drainage}}{t_{contact}}\right) \tag{4}$$

The drainage time $t_{drainage}$ has been expressed as the time required to squeeze out the fluid between particles from the separation at which the drainage law becomes relevant ($h_o \sim a/4$) to the critical separation, h_c. Together with the correlation $t_{contact} \sim \dot{\gamma}^{-1}$, the following expression for the estimation of the aggregation probability has been formulated:

$$P \sim (3Fl/4)^{-1/8} \tag{5}$$

where $Fl = 6\pi\eta\dot{\gamma}a^3/A_H$ is the flow number. In order to calculate the aggregation probability for our colloidal systems, we replaced the term a^3 by $2(a_p + a_i)a_p a_i$, to account for the aggregation between unequal particles. Increasing flow rate the aggregation probability, P, for a_p = 70 nm and a_i = 1 μm, is estimated to decrease from 39% at 23 mm^3/s, to approximately 23% at 1570 mm^3/s.

Another important aspect considering suspensions exposed to shear stress is the breakup of aggregates. In order to estimate the resistance of aggregates against breakage we estimated the Breakage number, as suggested by Xie et al. [28]. They expressed the
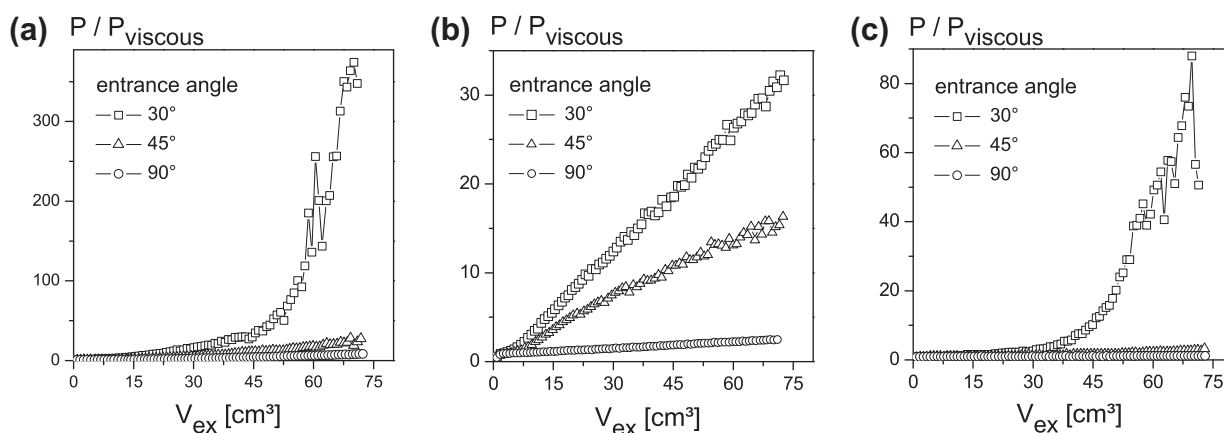
Fig. 13. Effect of the slit entrance angle on the flow-induced aggregation of the coarse pre-filtered PU dispersion at $\phi = 0.4$, $H = 26$ μm and flow rate = 63 mm^3/s (a), coarse pre-filtered polychloroprene dispersion at $\phi = 0.44$, $H = 11$ μm and flow rate = 63 mm^3/s (b) and coarse pre-filtered PS dispersion at $\phi = 0.47$, $H = 26$ μm and flow rate = 63 mm^3/s (c).

Breakage number as the ratio between shear energy and interparticle bonding energy. Considering a hetero-coagulation process, the Breakage number can be written in the following form:

$$\text{Br} = \left(\frac{\eta \dot{\gamma} (a_p + a_i) a_p a_i}{U_b} \right) \qquad (6)$$

where U_b is the interparticle bonding energy associated with the difference between the interaction energy barrier and the primary minimum. Details of U_b estimation can be found in [28]. The Br values calculated for $a_p = 70$ nm and $a_i = 1$ μm using Eq. (6) are 2 and 145 at 23 mm^3/s and 1570 mm^3/s respectively. Obviously, for primary particle and impurity sizes relevant for the investigated colloidal systems the Breakage number is always larger than unity and increases as the flow rate increases. Hence, for the experimental conditions in the ring-slit test, the applied shear energy is sufficient to overcome the interparticle bonding energy and the average aggregate size decreases as the shear energy or Breakage number increases. However, the aggregate breakage is a complex phenomenon which should be treated not only based on the concept of decreased aggregation efficiency but also large-scale defragmentation and so called surface erosion need to be considered. This is especially relevant for the extensional flow through the contraction region in our ring-slit die, which continuously accelerates and reaches the maximum elongation rate at the slit entrance. This means that the aggregates formed under low-strain conditions may breakup when exposed to the larger elongation rate in the proximity of the slit. Moreover, detailed considerations of multi-particle interactions would be necessary for a full quantitative description of flow-induced aggregation particularly for the case of highly concentrated suspensions investigated here.

Let us return to the results showing the effect of flow rate on the slit clogging phenomenon (Fig. 5). Based on the considerations discussed above we expect that the increase of the flow rate causes a decrease of the maximum aggregate size, which is controlled by the balance between flow-induced aggregation and breakage in the converging flow field at the slit entrance. This is supported by the data in Table 4 showing, that the volume fraction of the aggregates passed through the slit decreases with increasing flow rate.

4.5. Effect of slit entrance angle on flow-induced aggregation

To further investigate the effect of flow kinematics we studied the effect of the slit entrance angle on flow-induced aggregation. Fig. 13 shows the influence of the entrance angle for the three colloidal systems at 63 mm^3/s volumetric flow rate. The results for the PU and PS suspension are obtained at 26 μm slit height (Fig. 13a and c). Note that the samples are coarse pre-filtered before the ring-slit experiments. In the case of the polychloroprene suspension (fine pre-filtration) the slit height was fixed to 11 μm (Fig. 13b). The results presented in Fig. 13 shows a significant dependence of the normalized pressure drop on the slit entrance angle. For all colloidal systems, the pressure increase is most pronounced in the case of 30° slit entrance angle. In the case of PU and PS the results for 45° and 90° entrance angle almost superimpose, while in the case of the polychloroprene sample a continuous increase of the flow stability was detected with increasing the entrance angle. In order to understand the effect of slit entrance angle on the flow-induced aggregation we need to characterize the flow field in the ring-slit device. For this purpose we used the commercial CFD software Ansys Fluent 12. The 2D axisymmetric simulations were focused on the contracting region at the entrance of the slit with the following dimensions: $L' = 1.2$ mm, $L = 0.8$ mm, $H = 26$ μm and $\beta = 30°$, 45° and 90° (see Fig. 1b). The viscosity of the investigated shear-thinning suspensions is well described by the Carreau model, $\eta = \eta_\infty + (\eta_0 + \eta_\infty)(1 + (\lambda \dot{\gamma})^2)^{(n-1)/2}$. For calculations shown in Fig. 14 we have used the following model parameters determined for the PU dispersion with $\phi = 0.4$: $\eta_0 = 50$ Pas, $\eta_\infty = 0.006$ Pas, $\lambda = 75$ s and $n = 0.3$.
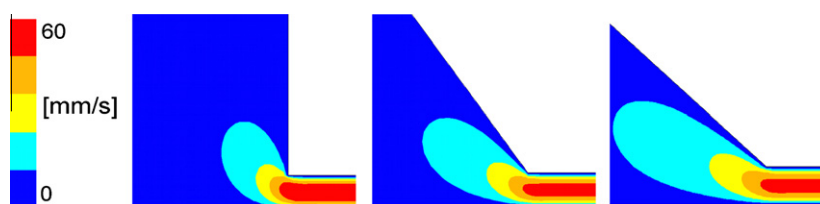

Fig. 14. Comparison of computed velocity field at $\beta = 90°$, 45° and 30° obtained with the following computation parameters: $L' = 1.2$ mm, $L = 0.8$ mm, $H = 26$ μm and flow rate 63 mm^3/s.

Furthermore, these simulations have been performed at the same flow rate (63 mm^3/s), as the experiments shown in Fig. 13, at which the flow is purely laminar (Re $\leqslant$ 0.15). The steady, laminar simulation models the piston movement using a velocity inlet. The pressure based Navier Stokes solver reproduces the pressure measurement data of the experiments.

Fig. 14 shows the flow velocity field in the slit entrance region for the 90°, 45° and 30° entrance angle. It can be seen that the region of velocity increase is enlarged in the case of 30° entrance angle in comparison with the steeper angles. Table 5 lists the maximal distance from the center of the slit entrance to the point of 20% and 40% of the maximal velocity for the three different entrance angles as calculated by the simulation. These regions are roughly comparable with the turquoise and yellow zones in Fig. 14. This shows that suspensions are exposed to a high-velocity field for longer time during the experiments with small entrance angles. A hypothesis could, thus, be that the increased flow stability with increasing slit entrance angle is due to a decreased residence time, i.e. time of exposure to the extensional flow field.

5. Conclusions

We have investigated the phenomenon of flow-induced aggregation in highly concentrated colloidal dispersions exposed to strongly converging flow fields. This phenomenon is relevant not only for classical technical operations like coating, pumping or filtration, but also for the application of concentrated suspensions in upcoming processing technologies based on microfluidic devices. In order to investigate this phenomenon experimentally, a ring-slit device has been developed which provides a strong flow contraction at the entrance of a narrow slit (10–25 µm) and allows for a variation of flow kinematics (slit height, entrance angle, length of converging entrance region and flow rate) in a wide range. Aggregates are not only formed in this microfluidic set-up, but are also detected via the increase in the extrusion pressure due to the gradual clogging of the slit entrance. Charge stabilized commercial polymer dispersions (PU, PS and polychloroprene) with a primary particle size of about 100 nm have been used here as model systems providing a shelf-life of at least 6 months. First of all we have shown that the pressure increase is not just due to the retention of pre-existing aggregates larger than the gap height. Experiments using a concentric cylinder shear cell reveal that aggregation does not occur in pure shear flow within the straight channel, and ring-slit tests with channels of different surface properties (hydrophilic vs. hydrophobic) indicate that clogging is not induced by the deposition of particles at the channel wall. Instead we have clearly shown that aggregation in the converging flow field at the slit entrance is the dominant effect leading finally to clogging of the slit. Accordingly, this phenomenon strongly depends on flow rate and for all investigated systems the slit clogs faster the lower the flow rate. This can be rationalized as follows. First, interparticle contact time is important for the formation of aggregates and the aggregation probability slightly decreases with increasing flow rate. Second, the dimensionless Breakage number, Br, is much larger than unity at all flow rates investigated here, thus aggregates may also be destroyed in the flow field and since Br increases with increasing flow rate clogging is slowed down as flow rate increases. Clogging is also more pronounced at lower entrance angles, we attribute this to a longer exposure of particles to high-velocity flow fields. The observed flow rate dependence also rules out hydrodynamic bridging as clogging mechanism. Ring-slit experiments with differently pre-filtered dispersions and experiments with added PMMA particles of different size and amount show that slit clogging is induced by the hetero-coagulation of primary nano-particles with micron-sized objects, which are essentially always present in commercial dispersions due to processing conditions. Only in the case of hetero-coagulation the critical Peclet number necessary to overcome the repulsive potential barrier between particles is exceeded. Hetero-coagulation can cause slit clogging even if the concentration of large particles is on the order of 100 ppm and the ratio of large particle size to gap height is <0.1. On the other hand, hetero-coagulation can be strongly influenced by the colloidal properties of the primary particles and strong differences in the ring-slit tests are observed for the PU, PS and polychloroprene dispersions under otherwise similar test conditions. Slit clogging can be suppressed even in the presence of large micron-sized particles by appropriate stabilization of the primary particles either by addition of a sufficient amount of surfactant providing full particle coverage or by an appropriate reduction in the ionic strength, which increases the range of electrostatic repulsion.

This work provides a sound experimental basis that clearly identifies the hetero-coagulation phenomenon as the elementary step in clogging of microchannels. However, we are still far from providing a quantitative interpretation and understanding of such complex systems as the highly concentrated commercial dispersions exposed to strongly converging flow fields that have been investigated here. But we can provide different strategies which offer improved processing stability. First, reduce the amount of micron-sized particles by using appropriate manufacturing conditions. Second, improve the colloidal stability of the primary nano-particles by appropriate surfactants or surface charge density. Finally, details of the flow kinematics also play a crucial role and appropriate design of processing equipment (gap dimensions, contraction angle) can provide stability. On the other hand, the addition of a small amount of micron-sized particles to a nano-particulate dispersion in combination with an appropriate design of the flow field might offer new options in soli-liquid separation technology.

Acknowledgments

References

[1] H.S. Chung, R. Hogg, Colloid Surf. 15 (1985) 119.
[2] W.B. Russel, D.A. Saville, W.R. Schowalter, Colloidal Dispersions, Cambridge University Press, Cambridge, 1989.
[3] P.C. Hiemenz, R. Rajagopalan, Principles of Colloid and Surface Chemistry, Taylor & Francis Group, 1997.
[4] G.R. Zeichner, W.R. Schowalter, J. Colloid Interface Sci. 71 (1979) 237.
[5] W.R. Schowalter, Ann. Rev. Fluid Mech. 16 (1984) 245.
[6] A.K. Chesters, Trans. Ind. Chem. Eng., Part I 69 (1991) 259.
[7] V. Oles, J. Colloid Interface Sci. 154 (1992) 351.
[8] J.C. Flesch, P.T. Spicer, S.E. AIChE J. 45 (2000) 1114.
[9] S.L. Elliott, R.J. Butera, L.H. Hanus, N.J. Wagner, Faraday Discuss. 123 (2003) 369.
[10] P. Sandkühler, J. Sefcik, M. Morbidelli, J. Phys. Chem. B 108 (2004) 20105.
[11] V. Lowry, M.S. Elaasser, J.W. Vanderhoff, A. Klein, C.A. Silebi, J. Colloid Interface Sci. 112 (1986) 521.
[12] Q. Wang, J. Colloid Interface Sci. 150 (1992) 418.
[13] M.R. Greene, D.A. Hammer, W.L. Olbricht, J. Colloid Interface Sci. 167 (1994) 232.
[14] G.R. Zeichner, W.R. Schowalter, AIChE J. 23 (1977) 243.
[15] R. Ettl, V. Schädler, N. Willenbacher, Nord. Pulp Pap. Res. J. 5 (2000).
[16] H.M. Wyss, D.L. Blair, J.F. Morris, H.A. Stone, D.A. Weitz, Phys. Rev. E 74 (2006).
[17] V. Ramachandran, H.S. Folger, J. Fluid Mech. 385 (1999) 129.
[18] C.W. Macosko, Rheology: Principles, Measurements and Applications, Wiley-VCH Publishers, Inc, 1994.
[19] E.E. Remsen et al., J. Electrochem. Soc. 153 (2006) G453.
[20] D. Dieterich, Prog. Org. Coat. 9 (1981) 281.
[21] R. Ranganathan, M. Petric, R. Medina, U. Garcia, B. Bales, Langmuir 17 (2001) 6765.
[22] R.J. Kuo, E. Matijevic, J. Chem. Soc. Faraday I 75 (1979) 2014.

[23] A. Zaccone, H. Wu, M. Lattuada, M. Morbidelli, J. Phys. Chem. B 112 (2008) 1976.

[24] A.R. Studart, E. Amstad, L.J. Gauckler, Langmuir 23 (2007) 1081.

[25] K. Holmberg, B. Jönsson, B. Kronberg, B. Lindman, Surfactants and Polymers in Aqueous Solution, John Wiley & Sons Ltd., West Sussex, 2003.

[26] A. Zaccone, H. Wu, D. Gentili, M. Morbidelli, Phys. Rev. E 80 (2009) 051404.

[27] J.E. Sader, S.L. Carnie, D.Y.C. Chan, J. Colloid Interface Sci. 171 (1995) 46.

[28] D. Xie, H. Wu, A. Zaccone, L. Braun, H. Chen, M. Morbidelli, Soft Matter 6 (2010) 2692.